

Preparation and Self-Assembly of Polyaniline Nanorods and Their Application as Electroactive Actuators

Seong Hun Kim,² Kyung Wha Oh,¹ Ji Hyoung Choi²

¹Department of Home Economics Education, Chung-Ang University, Seoul, Korea 156-756

²Department of Fiber and Polymer Engineering, Hanyang University, Seoul, Korea 133-791

Received 4 April 2008; accepted 8 October 2008

DOI 10.1002/app.31782

Published online 27 January 2010 in Wiley InterScience (www.interscience.wiley.com).

ABSTRACT: To improve the performance of ion-exchange polymer–metal composite (IPMC) actuators, an electrical pathway material for enhancing the surface adhesion between the membrane and the metal electrodes of the IPMC was studied. As an efficient electrical pathway material, polyaniline nanorods (PANI-NRs) doped with *p*-toluene sulfonic acid (TSA) were synthesized with a template-free method. The factors affecting polyaniline morphology were studied with various dopant concentrations and oxidant feeding rates. Highly conductive PANI-NRs were formed when they were synthesized with ammonium persulfate at a 5.0 mL/min oxidant feeding rate and doped with 0.125M TSA. The conductivity of the

PANI-NRs was 1.15×10^{-1} S/cm, and their diameters and lengths were 120–180 nm and 0.6–2 μ m, respectively. To apply the membrane as an actuator, perfluorosulfonated ionomer (Nafion)/PANI-NR blends were prepared by solution blending and casting. The actuating ability of the three-layered membrane consisting of Nafion/PANI-NR blends was then examined and compared with that of Nafion only. The actuating ability of the IPMC was improved when Nafion/PANI-NRs were used as electrical pathways. © 2010 Wiley Periodicals, Inc. *J Appl Polym Sci* 116: 2601–2609, 2010

Key words: conducting polymers; self-assembly; synthesis

INTRODUCTION

Conductive polymers have attracted considerable attention since doped polyacetylene was reported by Shirakawa et al. in 1977¹ because of their intrinsic one-dimensional conductivity and potential uses as electronic devices. Applications of these polymers include blends and coatings for electrostatic dissipation and electromagnetic interference shielding, electromagnetic radiation absorbers for the welding of plastics, and conductive layers for light-emitting polymer devices.^{2–12}

Among these conductive polymers, polyaniline (PANI) has special advantages, such as ease of synthesis, environmental stability, low cost of the monomer, nonredox doping by protonic acids, and ready modification of the oxidation states of the polymer chain.¹³ As the use of nanomaterials is expected to increase rapidly for biosensors, microelectronics, and photonics,^{14–16} many studies have focused on the synthesis and applications of nanoscale inorganic and organic materials. Template synthesis is a common and effective method for synthesizing the nano-

structures of conducting polymers.^{17,18} However, a template removal process is required to separate the synthesized nanotubes or wires. Therefore, it is particularly interest to form nanostructures by a self-assembly process, which does not require a tedious removal process. Recently, Wan and coworkers^{19–21} described a template-free method in the presence of β -naphthalene sulfonic acid as a dopant to synthesize microtubes of PANI. It was proposed that the formation of these PANI microtubes could be attributed to the self-assembly of β -naphthalene sulfonic acid molecules and their aniline salts into a microstructural intermediate,²² which acted as both a supermolecular template²³ and a self-doping agent. This indicated that the dopant used for self-assembling microtubes of PANI should have both doping and surfactant features, and these characteristics of the dopant contributed to the formation of various nanostructural morphologies.^{24–26}

Ion-exchange membranes are used in hydrogen fuel cells and in the production of sodium or potassium hydroxide.²⁷ They can also operate actuators when structured as metal–polymer–metal composite sheets. The ion-exchange polymer–metal composite (IPMC) actuator working in air is generally built in a configuration where the internal layer is a perfluorinated ionomer (Nafion) sandwiched between two metal electrode layers, and the relative differential expansion between the metal electrode layers causes bending.²⁸ IPMC actuators have several unique

Correspondence to: K. W. Oh (kwhaoh@cau.ac.kr).

Contract grant sponsor: Chung-Ang University (through research grants in 2009).

features: they can be operated with a relatively low voltage, and they can be used under water, which is useful in biomedical and marine applications.^{27,29} However, IPMC actuators have a small displacement (1.1 mm) and a low angular distance in water^{30,31} because IPMC has a low surface adhesion between the membrane and the metal electrodes, so the applied voltage is not effectively transmitted to membranes. Therefore, an electrical pathway between the membrane and the metal electrodes is required.

In this study, polyaniline nanorods (PANI-NRs) were synthesized with *p*-toluene sulfonic acid (TSA) as the dopant with a template-free method. The influence of the morphology was studied with various dopant concentrations and oxidant feeding rates; this enabled us to establish the process conditions for the formation of the PANI-NRs. In the application of the electrode for actuators, the perfluorosulfonated ionomer (Nafion)/PANI-NR blends were prepared by casting, and the actuating ability of a three-layered membrane, consisting of Nafion/PANI-NR blends, was estimated. The morphology, conductivity, and thermal stability of the PANI-NRs were investigated, and the actuating ability of the three-layered membrane actuator was compared with that of a pure Nafion membrane actuator.

EXPERIMENTAL

Synthesis of the PANI-NRs

PANI-NRs were synthesized by a template-free method with ammonium persulfate (APS) as an oxidant^{19–21} and TSA as a dopant. The aniline monomer was distilled under reduced pressure. A Nafion solution manufactured by DuPont (Wilmington, DE) and other reagents were used as received without further purification. All reagents were purchased from Aldrich (St. Louis, MO). The synthesis processes of the PANI-NRs with different dopant concentrations were as follows: 0.1 mol of aniline monomer was mixed with 1 L of distilled water containing TSA by stirring at room temperature; then, the mixture solution was kept in a cooling bath at -2°C during the synthesis process. The TSA concentrations were 0.0005, 0.005, 0.025, 0.075, 0.125, and 0.150M. APS (9.128 g) dissolved in 100 mL of deionized water was added slowly to the mixture solution, and the polymerization was conducted for 15 h.

Washing and drying of the PANI-NRs

We added an excess amount of methanol to the TSA-doped PANI-NR dispersion to precipitate PANI-NR powder by breaking the hydrophilic-lyophilic balance of the system and to stop the reaction.

The precipitates were collected with a glass filter and washed with methanol, ethyl ether, and deionized water three times to remove unreacted chemicals and aniline monomers. Then, the precipitate of the PANI-NRs was dried at room temperature *in vacuo* for 24 h. Finally, approximately 3 g of the PANI-NRs was obtained, which appeared as a dark green solid.

Preparation of the Nafion/PANI-NR blend film

The Nafion/PANI-NR blend was prepared by a solution-blending method. PANI-NRs (0.001 g) doped with 0.125M TSA were dissolved in *N,N*-dimethylformamide. This solution was blended with the 4 mL of a Nafion solution (5 wt %) containing aliphatic alcohol and water; then, the mixed solution was sonicated for 10 min. The Nafion/PANI-NR blend was poured into a casting frame. After the solvent was evaporated, the separated phase of the Nafion/PANI-NR films was produced. The viscous Nafion solution was painted on the surface of the Nafion/PANI-NR film and sandwiched with another Nafion/PANI-NR film; then, the three-layer laminated film was pressed. The pure Nafion film was prepared by the casting of the viscose Nafion solution.

Coating of the Ag electrode

Silver-mirror reaction solutions were prepared.²⁸ Solution 1 consisted of silver nitrate (0.6 g), 5.0N ammonium hydroxide (3.0 g), and deionized water (30.0 g). Solution 2 consisted of D-(+)-glucose (0.4 g), sodium hydroxide (0.8 g), and deionized water (20.0 g). The three-layer film was placed in solution 1 followed by the addition of solution 2. This process was repeated twice to produce better plating on the film surface. The silver-plated film was cut into strips $23 \times 2 \times 0.25 \text{ mm}^3$ (Length \times Width \times Thickness) and dried in the atmosphere for 1 day. Then, this film was immersed in a 0.1M LiCl solution for 6 h. The same process was conducted for the pure Nafion film to prepare the actuator.

Electrical conductivity measurement

The electrical conductivity of the PANI-NR powder was measured as follows: 0.02-g samples of PANI-NR with different TSA dopant concentrations were loaded into a 1.2-cm diameter pelletizer, and a pressure of 5 tons was applied for 2 min. Then, the electrical conductivity of the PANI-NR pellets was measured at room temperature with a four-probe technique with a Keithly 238 high-current-source measuring unit. All conductivity measurements

were performed in air by direct contact with the pellet's surface. The electrical conductivity of the samples was calculated as follows:

$$\sigma(\text{S/cm}) = \frac{1}{2\pi} \times \frac{I}{V} \quad (1)$$

where σ is the conductivity, s is the spacing between probes (0.3 cm), V is the voltage drop across the inner probes, and I is the current passed through the outer probes.

Characterization

Fourier transform infrared (FTIR) spectra of the PANI-NRs were recorded with a Nicolet 760 Magna IR spectrometer (Thermo Fisher Scientific, Inc., USA) with KBr discs. The morphology was confirmed by field emission scanning electron microscopy (FESEM, JEOL JSM-6330F, Tokyo, Japan) and transmission electron microscopy (TEM; JEOL JEM-2000).

Ultraviolet–visible (UV–vis) absorption spectra of the PANI-NRs in the 300–1000-nm range were recorded at room temperature with a Jasco FP-6500 (Tokyo, Japan). To record the spectra of the solutions, we used quartz infrasil cells with a 1-mm optical path, filled with a 0.01 wt % PANI-NR solution in *m*-cresol. Thermogravimetric analysis (TGA) of the PANI-NRs was carried out in a Pyris 1 thermogravimetric analyzer (Perkin Elmer, USA) under a nitrogen atmosphere at temperatures from 10 to 750°C at a heating rate of 10°C/min. The actuator performance was recorded with a digital camera, and the displacement, bending angle and curvature were calculated.

RESULTS AND DISCUSSION

Effect of the oxidant feeding rate

The effect of the oxidant feeding rate is shown in Figure 1. The PANI-NRs doped with TSA formed into agglomerated rod structures. The lengths of rods were short when the oxidant feeding rate was 2.5 mL/min because the first-aggregation rod-forming structures and secondary aggregation of PANI occurred almost simultaneously. Huang and Kaner³² reported the morphological evolution of PANI during chemical oxidative polymerization. Their PANI nanofibers formed at early stage in the polymerization process; however, as the process progressed, the nanofibers became scaffolds for the secondary growth of PANI and finally changed into irregularly shaped agglomerates containing nanofibers and particulates.

In this study, the oxidant feeding rate was controlled to suppress secondary aggregation and to in-

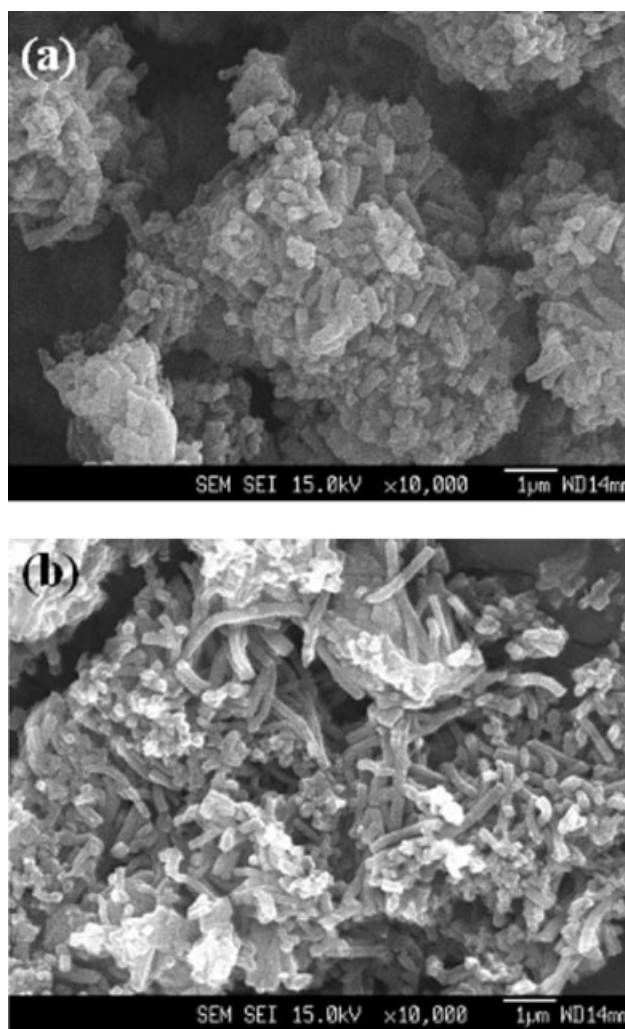


Figure 1 FESEM images of PANI-NRs doped with 0.1M TSA at different oxidant feeding rates: (a) 2.5 and (b) 5.0 mL/min.

crease the yield of PANI-NRs. As the oxidant was fed into the reaction at a feeding rate of 5.0 mL/min, the degree of agglomeration of the rod structures decreased, and the length of rods was increased. Under these process conditions, the rod formation reaction occurred, and secondary aggregation was effectively suppressed. The conductivities of PANI-NRs with different oxidant feeding rates were approximately the same ($\sim 10^{-1}$ S/cm); however, in the thermogram (Fig. 2), major weight losses were observed from 230–580°C because the thermal stability of the PANI-NRs formed with a feeding rate of 2.5 mL/min of APS was better than that of the PANI-NRs formed with a feeding rate of 5.0 mL/min. This was probably because of the aggregated structure of the PANI-NRs being more compact, which may have contributed to the better bonding of dopants and polymeric chains to each other. Despite this improved bonding, the PANI-

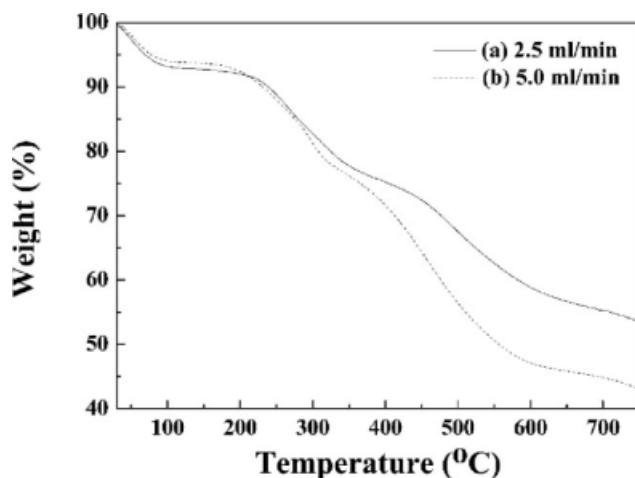


Figure 2 TGA thermograms of PANI-NRs at different oxidant feeding rates in a nitrogen atmosphere.

NRs had poor dispersability in the organic solvent. Therefore, the oxidant feeding rate was fixed at 5.0 mL/min for the following experiments.

Formation of the nanorods

The influence of the surfactant concentration on the morphology of the PANI nanostructures was investigated to form a self-assembled PANI-NRs. When TSA was used as the dopant and surfactant, micelles formed readily. At the same time, aniline may have existed in the form of anilinium salt or free aniline; therefore, the TSA and anilinium salt could form micelles, and free aniline diffused into their micelles.³³ Soluble free aniline or anilinium salt were

polymerized oxidatively by APS existing in the aqueous phase.³⁴ The reaction occurred mainly in the micelle–water interface adjacent to the surfactant head groups because hydrated APS molecules could not penetrate the micelle surface.³⁴ In the polymerization process, the micelles became spheres or rods, depending on the local conditions. In this study, two micelle types were observed. The morphology of synthesized PANI-NR powder with different dopant concentrations was confirmed, as shown in Figure 3, and their morphology was found to be significantly affected by the concentration of TSA. The variation in the morphology of the PANI-NRs of rod and grain was observed with increasing concentration of TSA. The rod morphology was initially formed in 0.0005M TSA, with its morphology being significantly exhibited from 0.025 to 0.125M TSA. The diameter and length of the rods was 120–180 nm and 0.6–2 μm . This was related to the hydrotropic behavior of TSA and the growth of nanorods. We assumed that the PANI aggregated in an orderly way and was gradually elongated in the micelles by sulfonic groups in the TSA.³⁵

However, the grain morphology was formed at a TSA concentration of 0.150M. This was probably because of the formation of PANI, in which an excess number of sulfonic groups interacted with each other and caused the elongation to be distributed by accretion.³⁶ Similar results were observed by Konyushenko et al.³⁷ when the polymerization of PANI was carried out in weak and strong acids. They concluded that a mildly acidic medium was favorable for the production of nanorods, but a

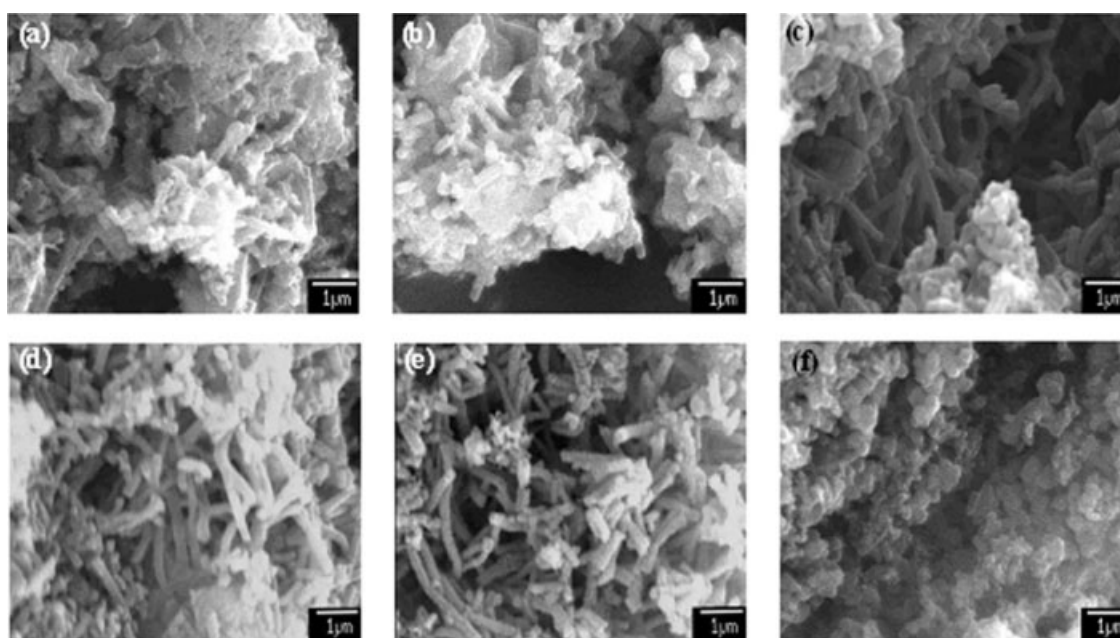


Figure 3 FESEM images of PANI-NRs doped with different TSA concentrations: (a) 0.0005, (b) 0.005, (c) 0.025, (d) 0.075, (e) 0.125, and (f) 0.150M.

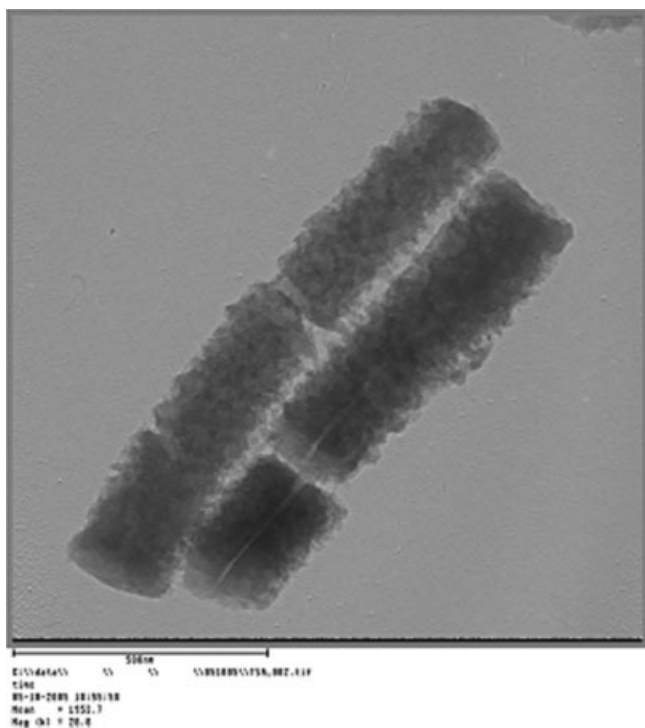


Figure 4 TEM images of PANI-NRs synthesized by a template-free method with APS at a 5.0 mL/min oxidant feeding rate and doped with 0.125M TSA.

granular morphology was produced in strongly acidic conditions because oligomer aggregation occurred in strong acidic conditions because of an increase in the hydrophobicity of aniline oligomers produced in the early stage of polymerization. However, at low pH's, the hydrophobicity of the oligomers of the early stage was reduced, and the oligomers became easily soluble and allowed the directional growth of PANI. Therefore, the PANI morphology was controlled by the concentration of the dopant and acidity of the reaction.

The morphology of the PANI-NRs synthesized by a template-free method with APS at a 5.0 mL/min oxidant feeding rate and doped with 0.125M TSA was also confirmed by TEM analysis, as shown in Figure 4.

Characterization of the PANI-NRs

The FTIR spectra of the PANI-NRs doped with different concentration of TSA are shown in Figure 5. All of the PANI-NRs showed characteristic peaks for the C=N=C quinoid ring at 1580 cm^{-1} , the C-N-C benzenoid ring at 1498 cm^{-1} , aromatic C-N at 1300 cm^{-1} , secondary C-N at 1140 cm^{-1} , SO_3^- at 657 cm^{-1} , and C-S at 600 cm^{-1} . The FTIR spectra of the PANI-NRs had no features in the region of $1750\text{--}3000\text{ cm}^{-1}$ because there were no functional groups in the PANI-NRs. These results indicate that the doping agent was sulfonic acid

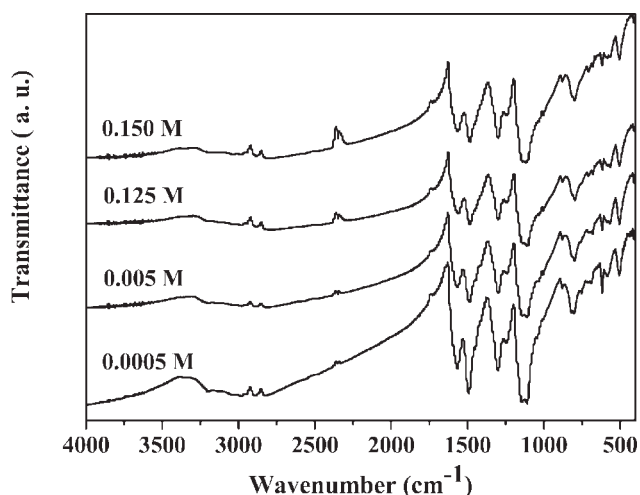


Figure 5 FTIR spectra of PANI-NRs doped with various TSA concentrations.

with benzene rings.^{38–40} All peaks appearing in the FTIR spectra of the PANI-NRs doped with different TSA concentration were identical. Their spectra were not shown and the peaks shifted; therefore, this indicated that the formation of rod structures was not a combination of other groups but an aggregation of PANI instead.

The UV-vis absorption spectra of the PANI-NRs dissolved in *m*-cresol solution were measured. As shown in Figure 6, polaron band transitions at about 400–420 and 820 nm were observed. The strong peak at about 400–420 nm was related to the partial protonation of PANI, whereas a broad peak with a long tail at 820 nm corresponded to the polaron band.^{41,42} Moreover, the peak intensity increased with an increase in the TSA concentration, which indicated that the doping level increased with an increase in the TSA concentration. In addition, the granular PANI formed with 0.15M TSA had a strong band at

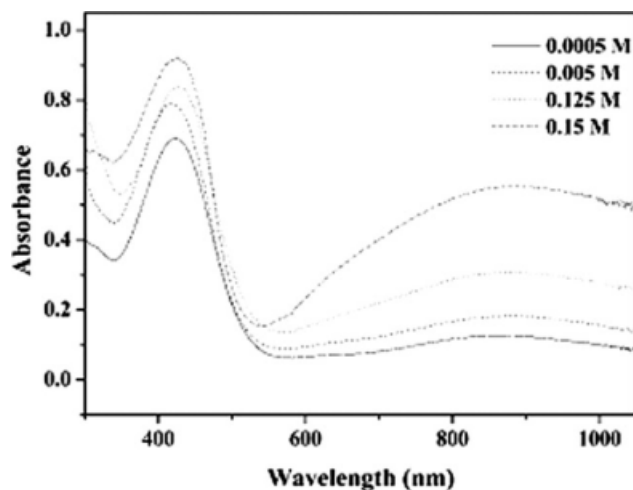


Figure 6 UV-vis spectra of PANI-NRs doped with various TSA concentrations.

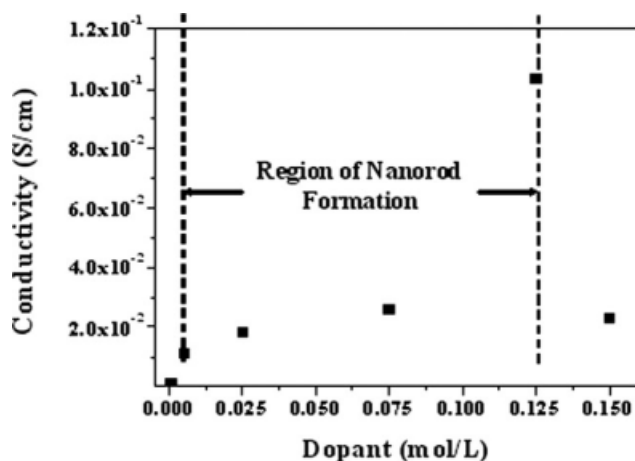


Figure 7 Electric conductivity of PANI-NRs doped with various TSA concentrations.

330 nm, which corresponded to the π - π^* transition of the benzenoid rings of PANI.⁴¹ However, this band did not appear in the nanorods. Therefore, we concluded that the electrical structure of the self-assembled PANI was slightly affected by its morphology.

The conductivities of the PANI-NRs doped with various TSA concentrations at room temperature are shown in Figure 7. The PANI-NRs had a conductivity within the range 10^{-2} to 10^{-1} S/cm, depending on the TSA concentration. The conductivity of the PANI-NRs increased as the TSA concentration increased from 0.0005 to 0.125M. However, the conductivity of PANI doped with 0.150M TSA decreased. In general, the conductivity of a conductive polymer is affected by the monomer/dopant molar ratio. The ideal molar ratio of monomer to dopant, that is, that having the highest conductivity, was found to be 2 : 1.⁴³ In our study, the highest conductivity of the PANI-NRs was found when their molar ratio was 2 : 1.06. This result was close to the ideal molar ratio. Furthermore, when the concentration of dopant was higher than the ideal molar ratio, the growth of chains was interrupted in aqueous solution, and the chain length was shortened. Therefore, their conductivity decreased with decreasing conductive path. In our polymerization process, PANI grain was obtained when it was doped with 0.150M TSA, and their conductivities were lower than those of PANI-NRs doped with 0.125M TSA. Another possible interpretation was in their morphological structures. The PANI-NRs had an approximately uniform morphology, whereas PANI grains lacked uniformity in their morphology. Therefore, we concluded that the PANI-NRs provided a higher conductivity than the PANI grains.

As shown in Figure 8, the thermal stabilities of the PANI-NRs were measured by TGA; the first weight

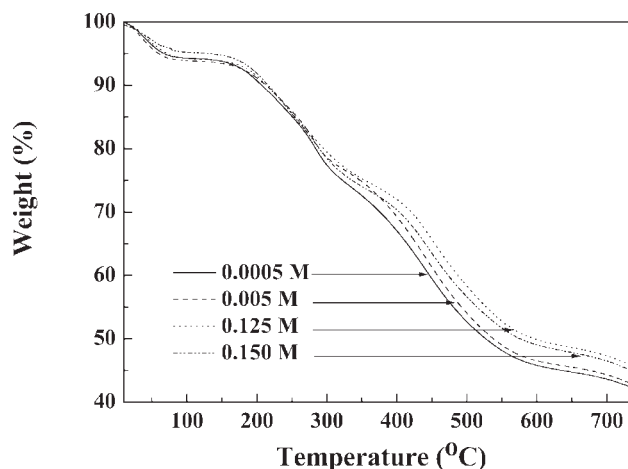


Figure 8 TGA thermograms of PANI-NRs (0.0005–0.125M) and PANI grains (0.150M) doped with various TSA concentrations in a nitrogen atmosphere.

loss was observed from 50 to 110°C and was attributed to the loss of water molecules.⁴⁴ The second weight-loss step occurred between 230 and 350°C, and this was attributed to the loss of unbound acidic dopant from the PANI-NR chain.⁴⁵ The third decomposition step region (340–580°C) indicated the degradation of the polymeric chain of the PANI-NRs.⁴⁵ The final step (>580°C) indicated the decomposition of the backbone and the ring opening of benzene for the PANI-NRs.⁴⁶

The analysis of the thermal degradation stability was performed by Doyle's method⁴⁷; the integral procedural decomposition temperature (IPDT) was calculated as follows:

$$\text{IPDT}(\text{°C}) = A^*K(T_f - T_i) + T_i \quad (2)$$

where A^* is the area ratio of the total experimental curve divided by the total TGA thermogram, K^* is the coefficient of A^* , T_i is the initial experimental temperature (°C), and T_f is the final experimental temperature (°C). The value of IPDT and its parameters are shown in Table I. IPDT of the PANI-NRs increased up to 0.125M TSA; however, IPDT of the grain structure was lower than that of the PANI-


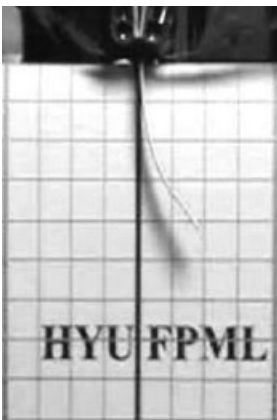
TABLE I
Thermal Stability Parameters for PANI-NRs and PANI Grains Doped with Various TSA Concentrations

TSA (mol/L)	A^*	K^*	IPDT (°C)
0.0005 ^a	0.698	0.478	253.9
0.005 ^a	0.706	0.488	261.4
0.125 ^a	0.726	0.497	273.5
0.150 ^b	0.720	0.493	269.1

^a PANI-NRs.

^b PANI grains was defined by SEM.

TABLE II
Actuation Performance of the Pure Nafion Membrane Actuator During Actuation in Air

Actuation performance			
			
			Average actuation performance
Applied voltage	+1.0 V	-1.0 V	±1.0 V
Bending angle	41.4°	45.6°	43.5°
Displacement	8 mm	9 mm	8.5 mm
Displacement per second	0.8 mm/s	1.2 mm/s	1 mm/s

NRs doped with 0.125M TSA. This indicated that the relatively homogeneous rod structures had a greater thermal stability than the grain structures.

Actuating ability

In the initial study, an actuator consisting of a pure Nafion membrane was prepared. The actuator visibly showed bending movements when a voltage was applied between the silver electrodes inserted into the Nafion membrane, as shown in Table II. The photographs showed that the actuator bent to the left, that is, to the side of the membrane layer, when +1.0 V was applied to the Nafion membrane and then bent back to the right when -1.0 V was applied to the bent actuator.

As shown in Figure 9, the bending angle [eq. (3)] and curvature [eq. (4)] of the actuator were calculated as follows:

$$\theta = \cos^{-1}\left(\frac{\overline{OB}}{R}\right) \quad (3)$$

$$\frac{1}{R} = \frac{2\delta}{\delta^2 + L^2} \quad (4)$$

where L is the length of the actuator, θ is the bending angle, δ is the displacement, and R is the curvature radius.

The bending angles of the left and right bending movements were 41.4 and 45.6°, their displacements were 8 and 9 mm, and the curvature values for the left and right were 0.029 and 0.034, respectively. The average performance values for the actuators were

43.5° of bending, 8.5 mm of displacement, and 0.032 of curvature. This was attributed to the movement of ionic clusters: when a voltage was applied, the ionic clusters in the Nafion membrane moved to a negatively charged electrode side, and then, the volume changed inside the Nafion membrane.⁴⁸

A three-layered membrane actuator was prepared with highly conductive PANI-NRs synthesized with APS at a 5.0 mL/min oxidant feeding rate and doped with 0.125M as an electrical pathway material. The performance of the actuator is shown in Table III. The actuator's measurement conditions were

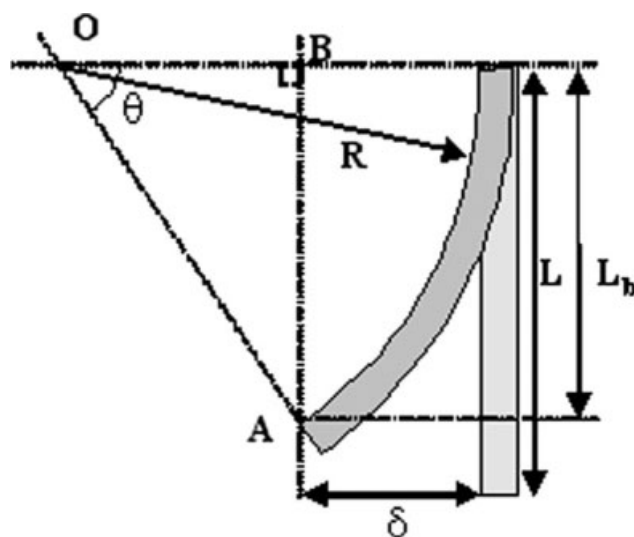
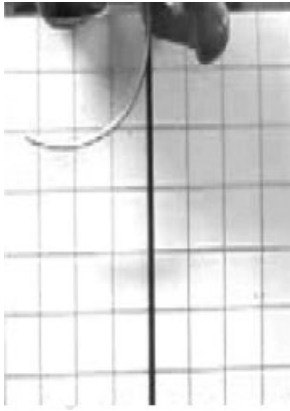
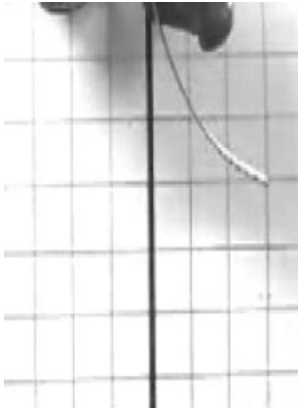


Figure 9 Schematic diagram of the actuating behavior (L = length of the actuator; θ = bending angle; δ = displacement; R = curvature radius).

TABLE III
Actuation Performance of the Three-Layered Membrane Actuator During Actuation in Air

Actuation performance			
			
			Average actuation performance
Applied voltage	+1.0 V	-1.0 V	±1.0 V
Bending angle	102.4°	62.3°	82.4°
Displacement	17 mm	15 mm	16 mm
Displacement per second	1.1 mm/s	0.8 mm/s	0.95 mm/s

the same as those of the pure Nafion membrane actuator. When +1.0 V was applied, the actuator bent to the left: its bending angle and displacement were 102.4° and 17 mm, respectively, and its curvature was 0.083 mm⁻¹. The actuator operated to the right when -1.0 V was applied to the bent actuator, and it had a 62.3° bending angle, a displacement of 15 mm, and a curvature value of 0.067. The three-layered membrane actuator exhibited an average bending angle of 82.4°, a displacement of 16 mm, and a curvature of 0.075 mm⁻¹. Therefore, the bending movement of the three-layered membrane actuator was better than that of the pure Nafion membrane actuator. We believe that the PANI-NRs performed as the primary electric pathway between the silver electrode and the membrane. The PANI-NRs permitted effective transmission of the applied voltage to the membrane and, thus, attracted lithium cation clusters.

CONCLUSIONS

PANI-NRs doped with various TSA concentrations were prepared by a template-free method. The oxidant feeding rate and TSA concentration affected on the morphology of the PANI-NRs. When the TSA concentration was in the range 0.005–0.125M, PANI-NRs with diameters of 120–180 nm and lengths of 0.6–2 μm were formed. When the feeding rate was 5.0 mL/min, the degree of agglomeration for rod structures was suppressed. The conductivity of PANI in the rod structure was higher than that in the grain structure. The thermal stability of the

PANI-NRs was improved with increasing TSA concentration up to 0.125M.

Highly conductive PANI-NRs were formed when they were synthesized with APS at a 5.0 mL/min oxidant feeding rate and doped with 0.125M TSA, and these were applied as actuator membranes. The Nafion/PANI-NR blends were prepared by solution blending and casting. The actuator consisting of the three-layered membrane had a higher angular distance and displacement than that of the pure Nafion membrane. It appeared that the PANI-NRs may have reacted to the conductive pathway between the metal electrode and membrane when a voltage or current was applied, which resulted in the efficient attraction of lithium cation clusters. Consequently, PANI-NRs may be applied to conductive fillers for functional polymer blends with high conductivities and thermal stabilities.

References

- Shirakawa, H.; Louis, E. J.; MacDiarmid, A. G.; Chiang, C. K.; Heeger, A. J. *J Chem Soc Commun* 1977, 577.
- Kohlman, R.; Joo, J.; Epstein, A. J. *Physical Properties of Polymers Handbook*; AIP: New York, 1996; Chapter 34, p 453.
- Epstein, J. *Conductive Polymers and Plastics in Industrial Applications*; Plastics Design Library: Washington, DC, 1999.
- Kohlman, R.; Epstein, A. J. *Handbook of Conducting Polymers*; Marcel Dekker: New York, 1997; p 85.
- Wallance, G. G.; Spinks, G. M.; Kane-Maguire, L. A. P.; Teasdale, P. R. *Conductive Electroactive Polymers: Intelligent Materials Systems*; CRC: New York, 2003; Chapter 1, p 1.
- Oh, K. W.; Kim, S. H.; Bahk, J. H. *J Korean Fiber Soc* 2002, 39, 757.
- Jang, S. H.; Byun, S. W.; Kim, S. H.; Joo, J. S.; Lee, J. Y.; Jeong, S. H. *J Korean Fiber Soc* 2002, 39, 217.
- Kaynak, A. *Fiber Polym* 2001, 2, 171.

9. Kaynak, A.; Wang, L.; Hurren, C.; Wang, X. *Fiber Polym* 2002, 3, 24.
10. Oh, K. W.; Park, H. J.; Kim, S. H. *J Appl Polym Sci* 2003, 88, 1225.
11. Oh, K. W.; Park, H. J.; Kim, S. H. *J Appl Polym Sci* 2004, 91, 3659.
12. Kim, S. H.; Oh, K. W.; Bahk, J. H. *J Appl Polym Sci* 2004, 91, 4064.
13. Skotheim, T. A. *Handbook of Conducting Polymers*; Marcel Dekker: New York, 1986; Vol. 1, p 2.
14. Bachtold, A.; Hadley, P.; Nakanishi, T.; Dekker, C. *Science* 2001, 294, 1317.
15. Riehn, R.; Charas, A.; Morgado, J.; Cacialli, R. *Appl Phys Lett* 2003, 82, 526.
16. Subramanian, A.; Oden, P. I.; Kennel, S. J.; Jacobson, K. B.; Warmack, R. J.; Thundat, T.; Doktycz, M. J. *Appl Phys Lett* 2002, 81, 385.
17. Penner, R. M.; Martin, C. R. *J Electrochem Soc* 1986, 133, 2206.
18. Cai, Z.; Martin, C. R. *J Am Chem Soc* 1989, 111, 4138.
19. Wan, M. X.; Liu, J.; Qiu, H. J.; Li, J. C.; Li, S. Z. *Synth Met* 2001, 119, 71.
20. Qiu, H. J.; Wan, M. X. *Macromolecules* 2001, 34, 675.
21. Wei, Z. X.; Zhang, Z. M.; Wan, M. X. *Langmuir* 2002, 18, 917.
22. Wan, M. X.; Li, J. *J Polym Sci Part A: Polym Chem* 2000, 38, 2359.
23. Beginn, U. *Adv Mater* 1998, 10, 1391.
24. Ciesla, U.; Schuth, F. *Micropor Mesopor Mater* 1999, 27, 131.
25. Bockstaller, M.; Kohler, W.; Wegner, G.; Vlassopoulos, D.; Fytas, G. *Macromolecules* 2000, 33, 3951.
26. Kinlen, P. J.; Liu, J.; Ding, Y.; Graham, C. R.; Remsen, E. E. *Macromolecules* 1998, 31, 1735.
27. Enikov, E. T.; Seo, G. S. *Sens Actuators A* 2005, 122, 264.
28. Tamagawa, H.; Nogata, F.; Watanabe, T.; Abe, A.; Yagasaki, K.; Jin, J. Y. *J Mater Sci* 2003, 38, 1039.
29. Bar-Cohen, Y. *Electroactive [EAP] Actuators as Artificial Muscles*; SPIE: Washington, DC, 2001.
30. Abe, Y.; Mochizuki, A.; Kawashima, T.; Yamashita, S.; Asaka, K.; Oguro, K. *Polym Adv Technol* 1998, 9, 520.
31. Vidal, F.; Plesse, C.; Teyssie, D.; Chevrot, C. *Synth Met* 2004, 142, 287.
32. Huang, J.; Kaner, R. B. *Angew Chem Int Ed* 2004, 43, 5817.
33. Zhang, Z.; Wei, Z.; Wan, M. *Macromolecules* 2002, 35, 5937.
34. Xia, H.; Wang, Q. *Chem Mater* 2002, 14, 2158.
35. Ajayan, P. M.; Iijima, S. *Nature* 1993, 361, 333.
36. Tang, B. Z.; Xu, H. *Macromolecules* 1999, 32, 2569.
37. Konyushenko, E. N.; Stejskal, J.; Sedenkova, I.; Trchova, M.; Sapurina, I.; Cielar, M.; Prokes, J. *Polym Int* 2006, 55, 31.
38. Cruz-Estrada, R. H.; Folkes, M. J. *J Mater Sci* 2000, 35, 5065.
39. Davies, S. J.; Ryan, T. G.; Wilde, C. J.; Beyer, G. *Synth Met* 1995, 69, 209.
40. Hsu, W. P.; Ho, K. S. *J Appl Polym Sci* 1997, 66, 2095.
41. Zang, L.; Wan, M. *Thin Solid Films* 2005, 477, 24.
42. Huang, J.; Wan, M. *J Polym Sci Part A: Polym Chem* 1999, 37, 151.
43. Fan, J.; Wan, M.; Zhu, D. *Solid State Commun* 1999, 110, 57.
44. Matveeva, E. S.; Callejak, R. D.; Martinez, E. S. *Synth Met* 1994, 67, 207.
45. Boyle, A.; Penneau, P. F.; Genies, E. M.; Rieckel, C. J. *J Polym Sci Part B: Polym Phys* 1992, 30, 265.
46. Yang, C. M.; Chen, C. Y. *Synth Met* 2005, 153, 133.
47. Doyle, C. D. *Anal Chem* 1961, 33, 77.
48. Kim, K. J.; Shahinpoor, M. *Polymer* 2002, 43, 797.